Discovery of new thermal anomalies in trehalose dihydrate: insights into their properties through differential scanning calorimetry and microscopic observation

Reon Oka[1] · Taisei Yato[1] · Keisuke Yamakawa[1] · Haruhiko Yao[1] · Soichi Tatsumi[1]

Abstract

We have investigated the thermal properties of trehalose dihydrate by using differential scanning calorimetry and direct observation by optical microscope. A key result of our findings is the discovery of thermal anomalies around 350 K (LTA) and 430 K (HTA) for liquidous trehalose dihydrate and confirm the relation between those anomalies. By connection with microscopic observation and DSC curves, we have found that the emergence of small crystalline structures above the melting point of trehalose dihydrate plays an important role in understanding LTA and HTA. LTA corresponds to the growth process for this structure, while HTA is a gradual melting procedure.

Keywords Cryptobiosis · Differential scanning calorimetry · Optical observation

Introduction

Trehalose is a disaccharide formed by the glycosidic linkage of glucose and is found everywhere within many plants, animals, fungi, algae, etc. Its high ability to retain water helps trehalose to be utilized in many fields, such as skin toner and food [1–3]. Among them, we focus on its association with a survival strategy called cryptobiosis observed in certain microorganisms. For example, the larvae of the polypedilum vanderplanki are known to replace the water in their bodies with trehalose under extremely arid conditions [4–6]. Then, the larvae of the polypedilum vanderplanki can withstand temperatures up to 350 K for a short period in the cryptobiosis state [4]. Sakurai et al. proposed a hypothesis to explain this phenomenon based on the amorphous state of the trehalose. They claim that amorphized trehalose preserves the biological tissue at lower temperatures while at a temperature larger than 350 K, this mechanism does not work since the trehalose experiences the glass transition and then turns to be liquid state [5, 6].

The proposed mechanism to preserve biological tissues owing to the amorphized trehalose seems to be reasonable; however, its invalidation procedure needs to take much more attention concerning the water content of the system. Owing to the high ability of water retention of trehalose, even under arid conditions, the system contains water to some extent. From that standpoint, we would like to point out the tremendously large glass transition temperature reported which needs to be considered. According to the literature, the glass transition of dried larvae, which should have originated from contained trehalose, is about 338 K [5]. With consulting the relation between the glass transition temperature and water content of the trehalose hydrate [7–11], this corresponds to the trehalose hydrate with a hydration amount of 4 mass% while the reported hydration amount in the same literature is about 10 mass% [5].

It should be noted that this estimate does not exclude water hydrates other than trehalose. However, it is important to note that the hydration amount of 10 mass% roughly

✉ Soichi Tatsumi
statsumi@kit.ac.jp

Reon Oka
m2672008@edu.kit.ac.jp

Taisei Yato
m9672029@edu.kit.ac.jp

Keisuke Yamakawa
m6617022@edu.kit.ac.jp

Haruhiko Yao
hyao@kit.ac.jp

[1] Department of Macromolecular Science and Engineering, Kyoto Institute of Technology, Hashiue-cho, Matsugasaki, Sakyo-ku, Kyoto, Kyoto 606-8585, Japan

corresponds to trehalose dihydrate. A comprehensive study on the amorphous state of trehalose hydrate has shown that trehalose dihydrate exists stably under a wide range of temperature and humidity conditions around room temperature [12]. The work done by Sakurai et al. is in the areas covered there.

Based on the above considerations, we comprehensively investigated the thermophysical properties of trehalose dihydrate, which exists stably in its natural state, to understand that cryptobiosis is invalidated at high temperatures. As a result, we discovered two thermal anomalies in trehalose dihydrate. They exist at around 350 K (low-temperature anomaly, LTA) and around 430 K (high-temperature anomaly, HTA), respectively. Here, LTA in particular is very close to the temperature at which cryptobiosis is invalidated. Here, we report the results of the investigation of LTA and HTA through thermal measurements by using differential scanning calorimetry (DSC) and direct observation using a microscope.

Materials

In this experiment, we used trehalose dihydrate with a purity of larger than 98% supplied from FUJIFILM Wako Pure Chemical Corp. as purchased. Its molecular weight, melting temperature, glass transition temperature, and mass fraction of water are 378.33 g mol^{-1}, 370 K, 253 K, and 9.52 mass%, respectively. On the other hand, the melting temperature and glass transition temperature of anhydrous trehalose are 487 K and 388 K, respectively. As shown in the literature [7],

temperatures of melting point and glass transition of trehalose hydrate are very sensitive to the amount of hydration.

Methods

Differential scanning calorimetry (DSC)

A TA2920 differential scanning calorimeter with a Refrigerated Cooling System was used to assess the thermal properties of trehalose dihydrate. Samples were equilibrated around room temperature and scanned between 250 and 450 K, with a scanning rate of 5 K min^{-1} and nitrogen flow rate of 30 mL min^{-1}. All measurements introduced in this report involve corresponding temperature profiles with each figure. The temperature calibration with water, trehalose dihydrate, and anhydrous trehalose was achieved. At higher than the melting point of trehalose dihydrate, the part of water molecules is no longer constrained to trehalose and make increase the internal pressure of the sample cell. In this experiment, we used a pressure-resistant sample pan up to 5.0 MPa to make the system closed by preventing the destruction of the sample cell.

Microscopic observation

An optical microscope (Nikon, OPTIPHOT-2) was used to investigate morphological changes accompanied by melting, LTA, and HTA. The schematics of the experimental setup are shown in Fig. 1. As shown in Fig. 1b, the sample was thinly sandwiched between two cover glasses
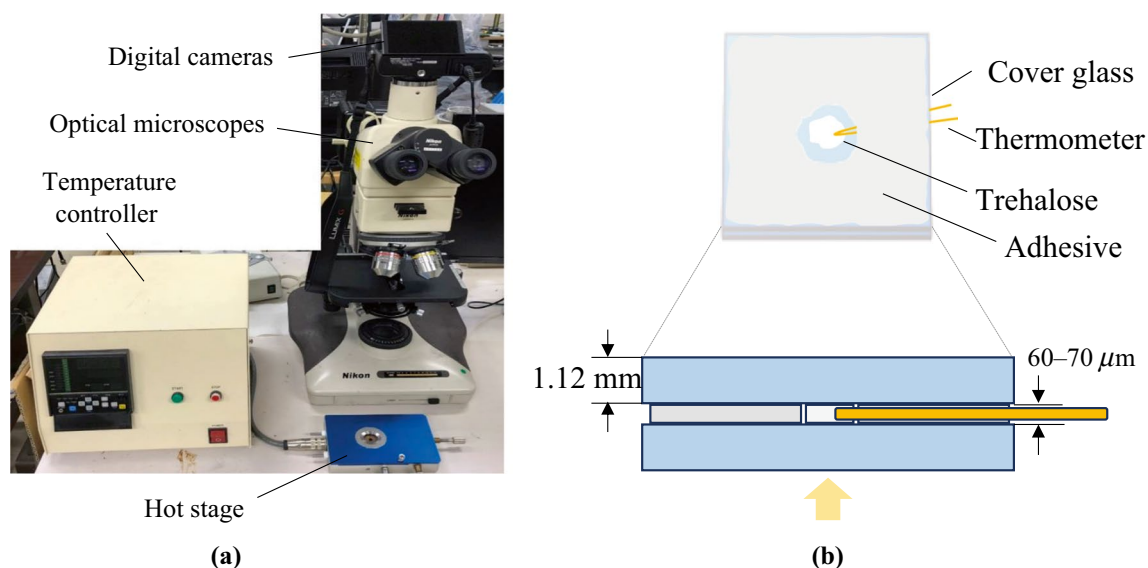

Fig. 1 Schematics of **a** experimental setups for microscopic observations and **b** preparation of sample cell. The yellow arrow in Fig. (**b**) indicates the direction to observe by using a microscope. (Color figure online)

Fig. 2 Schematics of curve with completion of HTA (**a**) and without completion of HTA (**c**). **b** and **d** indicate the temperature profiles of (**a**) and (**c**), respectively. Results only for heating scans are shown. Black, red, green, and blue lines indicate first, second, third, and fourth heating scans, respectively. (Color figure online)
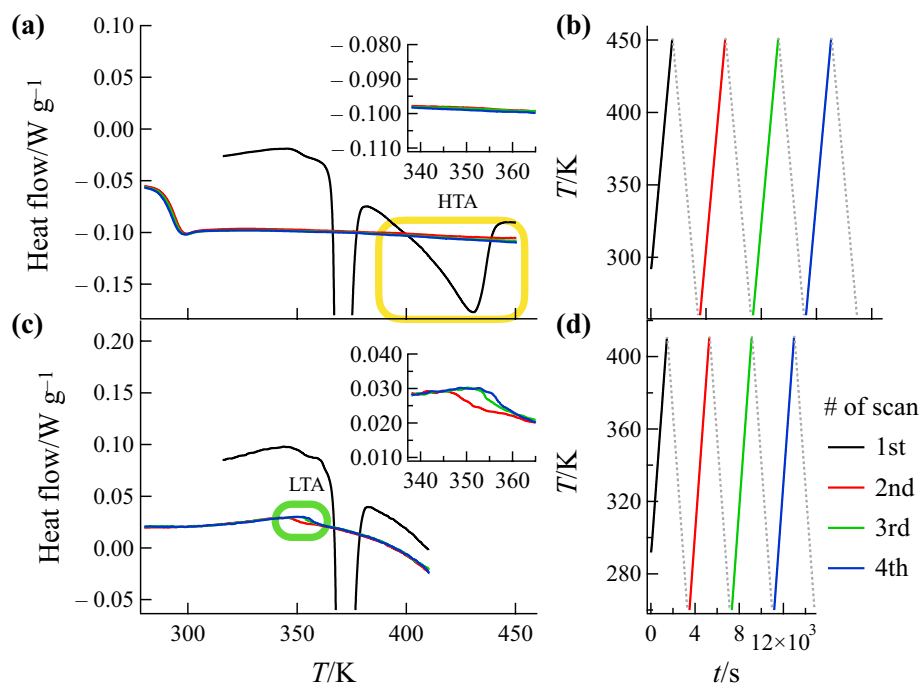
with a thickness of about 1.12 mm, and the area around the sample was firmly solidified with adhesive to form a sample cell. This prevents the cell from being destroyed by high pressures above the melting point of trehalose dihydrate. As shown in Fig. 1b, the thermometer is placed at nearby the sample. The K-type thermocouple was used to measure the temperature of the sample. Finally, the thickness of the sample was approximately 60–70 μm.

The sample cell was installed into the temperature-controlled stage. A digital camera (Panasonic, DMC-GX7MK2) through the optical microscope was used to monitor the morphological changes during the temperature scan. The range of temperatures to scan is from 320 to 470 K. Then, the outcome of the scanning rate is about 1 K s^{-1}. The agreement between the temperature measured by the thermometer and the sample temperature is confirmed by using the melting of trehalose dihydrate. Corresponding temperature profiles are shown in each figure.

Results

Findings of LTA and HTA

Figure 2 shows the summary of our findings of two thermal anomalies of trehalose dihydrate. The first heating run as shown in Fig. 2a, c indicates the melting of crystalline trehalose dihydrate. While the curve shown in Fig. 2a stops the temperature scan at around 450 K, Fig. 2c goes around 410

K. The consequent runs of them and indicates the thermal properties of liquid trehalose dihydrate. The inset of Fig. 2c represents the LTA of liquid trehalose dihydrate with an effect of repetition of measurements. As shown in this figure, with repetition of the temperature scan, LTA is shifted to the higher temperature. The inset of Fig. 2a demonstrates the disappearance of LTA with the completion of HTA. Another significant difference between Fig. 2a, c is the existence of the glass transition around 295 K. Figure 2a represents the existence of the glass transition around 295 K with completion of HTA, while no glass transition has appeared above 270 K without completion of HTA (Fig. 2c). With consideration of the relation between glass transition temperature and the degree of hydration for trehalose, the fraction of water of trehalose hydrate in Fig. 2a corresponds to 1.4 water molecules against 1 trehalose. Here, different from glass transition or phase transition phenomena, both LTA and HTA only appeared at a heating run. To be noted, this work is the first case to report LTA in trehalose dihydrate.

The effect of repetition and annealing on LTA

To examine the repetition effect as shown in Fig. 2c, a further repetitive experiment from 250 to 390 K has been conducted. Figure 3b represents the summary of the curve done by those experiments. To quantify the temperature at which LTA occurs, we extrapolated the heat flow on the low-temperature side and the high-temperature side, as shown in Fig. 3c, and defined the intersection with the median of both extrapolated curves and experimental results as T_X. As

Fig. 3 The summary of repetitive experiments from 250 to 390 K. **a** represents the temperature profile for this run. **b** represents each curve around LTA. With increasing the number of repetitions, the position of LTA is shifted to a higher temperature. **c** represents schematics to get temperatures for the occurrence of LTA (T_X). Black lines represent the extrapolation of curves for lower temperature, higher temperature, and the average of both, respectively. The red line represents the raw curve. **d** represents repetition number dependences for T_X. (Color figure online)
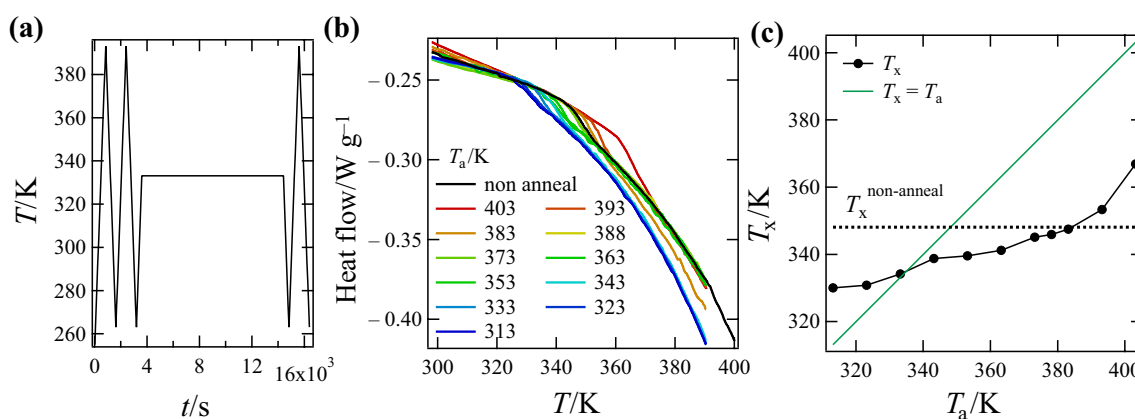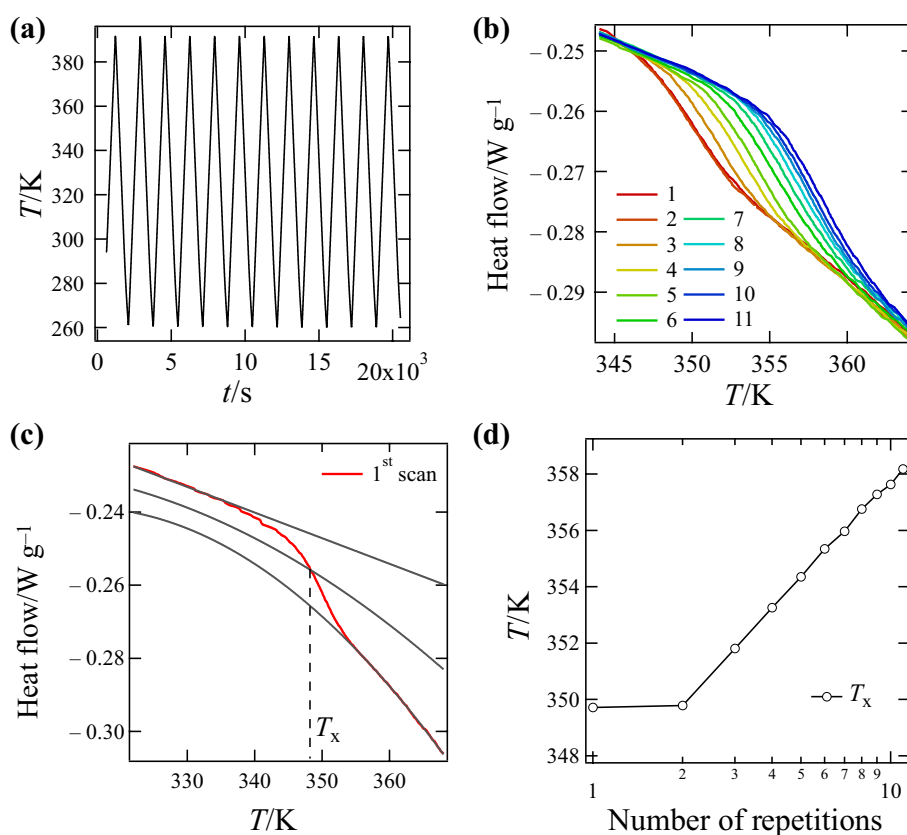

Fig. 4 The summary of annealing experiments with the T_a ranging from 313 to 403 K. **a** represents the schematic of the temperature profile. **b** represents the summary of curves around LTA. With increasing the T_a, T_X is shifted to a higher temperature. **c** represents the T_a dependencies of T_X. The green line indicates $T_X = T_a$ and the dashed line indicates the T_X for a non-annealing sample. (Color figure online)

shown in Fig. 3d, T_X shifts toward the higher temperature in proportion to the logarithm of the number of repetitions. For the elucidation processes for T_X, the curve of the low-temperature side is fitted by a linear function and that of the high-temperature side is fitted by a quadratic function.

The results of repetitive measurements suggest that T_X is influenced by the time to experience higher temperatures. To verify how the LTA changes by annealing, the annealing

effect with changing annealing temperature is examined. An overview of this procedure is shown in Fig. 4. Obtained curves with annealing treatment sandwiched between repeated measurements from 250 to 390 K are shown in Fig. 4b. The annealing time is fixed at 3 h, and the annealing temperature, T_a, is varied in the range of 313–403 K. The typical temperature profile of this measurement is shown in Fig. 4a. As a result, the higher the T_a, the higher the T_X and

Fig. 5 The morphological change during the melting of trehalose dihydrate. **a** represents the temperature profile. The red dot with the alphabet indicates the point to take a snapshot shown in (**b**–**e**). The blue dashed line indicates the melting temperature of trehalose dihydrate. **b** indicates the snapshot of the crystalline structure of trehalose dihydrate. **c** represents the snapshot just after the melting transition. **d**, **e** represent the emergence of the spike-like crystalline structures and the increase of those, respectively. **f** represents the result for figure analysis in each temperature. Red dashed squares with numbering (i), (ii), and (iii) correspond to the region to show the close-up shown in (**f**). Each region corresponds to the local peak in the profiles shown in (**f**). (Color figure online)
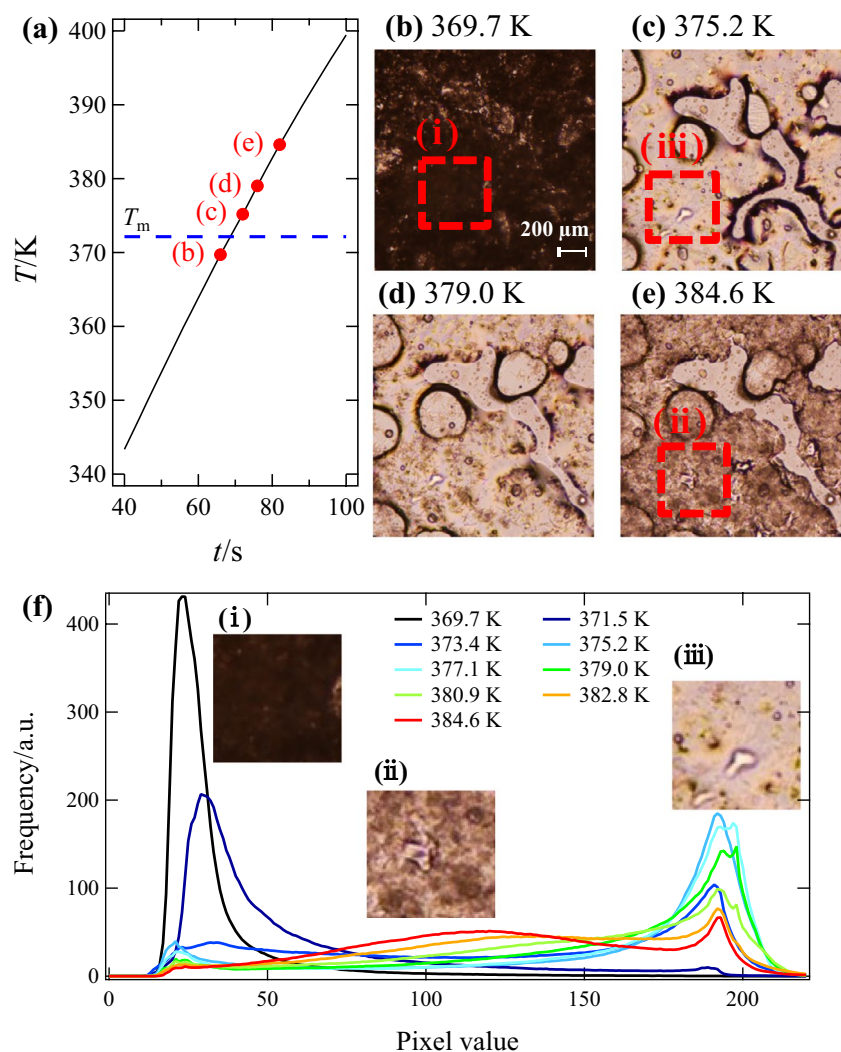
the larger the strength of LTA. Figure 4c summarizes the dependence of T_X on T_a. The dashed line shows the T_X for no annealing sample, which almost matches the results with $T_a = 378$ K. It should also be pointed out that T_a and T_X are reversed at 333 K. In particular, with consideration of the normal annealing effect to erase thermal anomalies lower than T_a, it is a little strange that the T_X is lower than the T_a when the T_a is 333 K or higher. It suggests that LTA cannot be treated in the same way as a normal thermal anomaly shown in other systems.

Morphological changes with melting transition of trehalose dihydrate

Figure 5 shows the results of direct observation using a microscope to capture the morphological changes accompanied by the occurrence of melting transition of trehalose dihydrate. Firstly, reflecting the existence of the crystalline structures of trehalose dihydrate, Fig. 5b looks dark due to

diffuse reflection from powdered trehalose dihydrate. Then, bypassing the melting point, trehalose dihydrate was liquified and the system turned to be uniform, as shown in Fig. 5c. However, with a slight increase in the temperature, the spike-like microcrystalline structures appeared (Fig. 5d), and the number of those increases with increasing temperature (Fig. 5e). Those relationships become significant by focusing on the difference in brightness between (i) the crystalline structures of trehalose dihydrate, (ii) the microcrystals formed after melting, and (iii) the liquid state. Figure 5f is obtained by counting the number of pixels as a function of brightness, namely, pixel value. With meeting the expectation, the obtained profiles show three local peaks reflecting the three different states.

Profiles in Fig. 6 provide the close-up of profiles as shown in Fig. 5f. Frequencies around the pixel value of 120 indicate the amount of the microcrystals after melting (Fig. 6a). An increase in the amount of microcrystals is observed with the temperature rise. Conversely, frequencies around the

Fig. 6 The close-up of profiles for the figure analysis with changing temperature for Fig. 5f is shown. **a** and **b** represent profiles around pixel values of 120 (**a**) and 190 (**b**), respectively. (Color figure online)
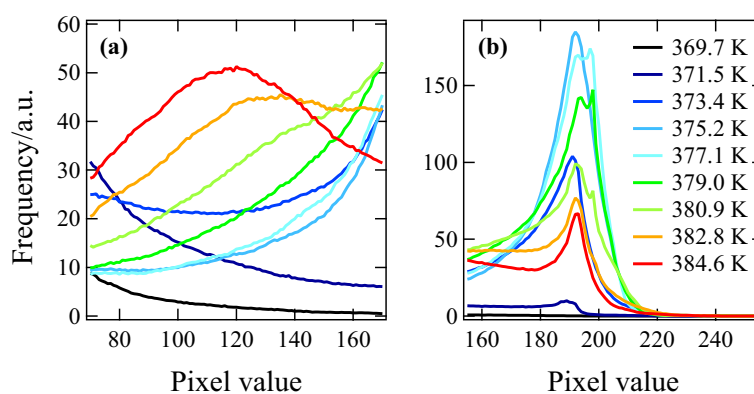

Fig. 7 The morphological change accompanied by the occurrence of HTA is shown. The upper panel represents the temperature profile with the whole microscopic observation. The red-dotted region indicates the first heating scan for observing the melting of trehalose dihydrate, which corresponds to Fig. 5. The blue-dotted region indicates the second heating scan for observing morphological change in LTA, which corresponds to Fig. 8. The green region indicates the occurrence of HTA. Alphabets shown in the upper panel indicate points to obtain snapshots shown in (**a**–**i**), respectively. Figures **a**–**e** represent the snapshot before completion of HTA and Figs. **f**–**i** represent the snapshot after completion of HTA. (Color figure online)
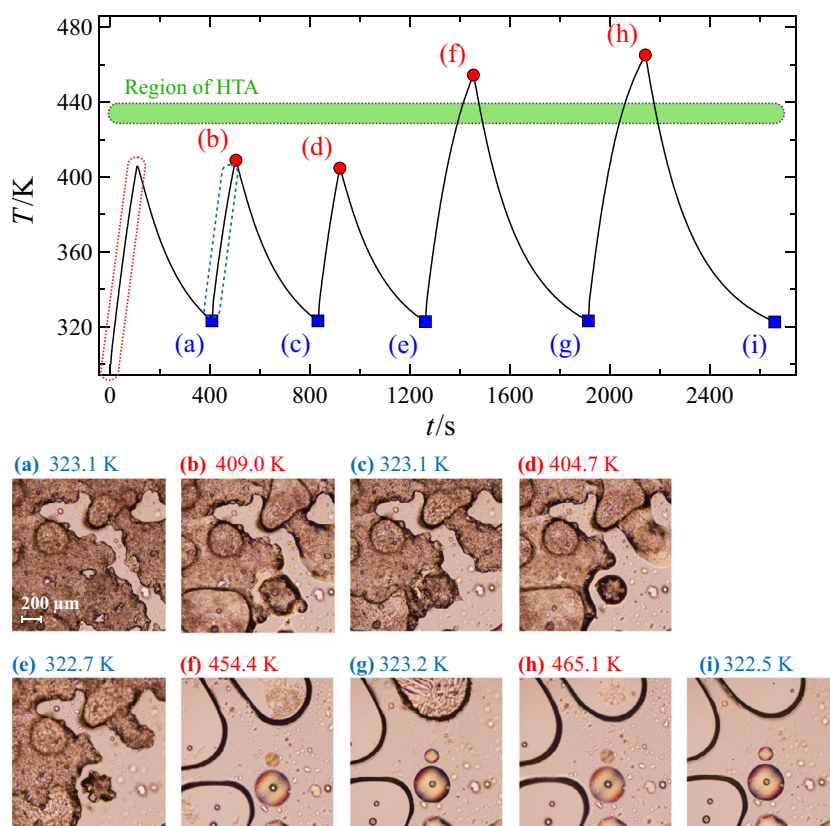

pixel value of 190 represent the amount of the liquid state (Fig. 6b). There is a rapid increase after the melting point (370 K), followed immediately by a drop with the increase of microcrystals.

Morphological changes throughout whole process focusing with HTA

An overview of the morphological changes after melting is given in this section with paying attention to whether HTA has been completed. In the previous section, we introduced the formation of microcrystals after melting. As shown in

Fig. 7, trehalose dihydrate was firstly heated to about 410 K and lowered the temperature. Then, we investigated morphological changes caused by the repetition of temperature scans. Figure 7a–i shows snapshots taken at the lowest and highest temperatures for each temperature scan. Including the first heating for melting, maximum temperatures were around 410 K up to the third heating. Since 410 K is below the temperature at which HTA occurs, snapshots show the existence of many microcrystals (Fig. 7a–e). On the other hand, from the fourth scan, since the maximum temperatures rose to over 450 K, which is higher than 440 K, where HTA occurs, the microcrystals disappeared and the entire

Fig. 8 The morphological change during LTA. **a** represents the temperature profile. The red dot with the alphabet indicates the point to take a snapshot shown in **b–d**. The blue-dashed line indicates the temperature for LTA. **b** indicates the snapshot just after finishing first scan. **c** represents the snapshot just before LTA. **d** represents the snapshot just after LTA. **e** represents the result for figure analysis in each temperature. White-dashed squares with numbering (i), (ii), and (iii) correspond to the region to show the close-up shown in (**e**). Each region corresponds to the local peak in the profiles shown in (**e**). (Color figure online)
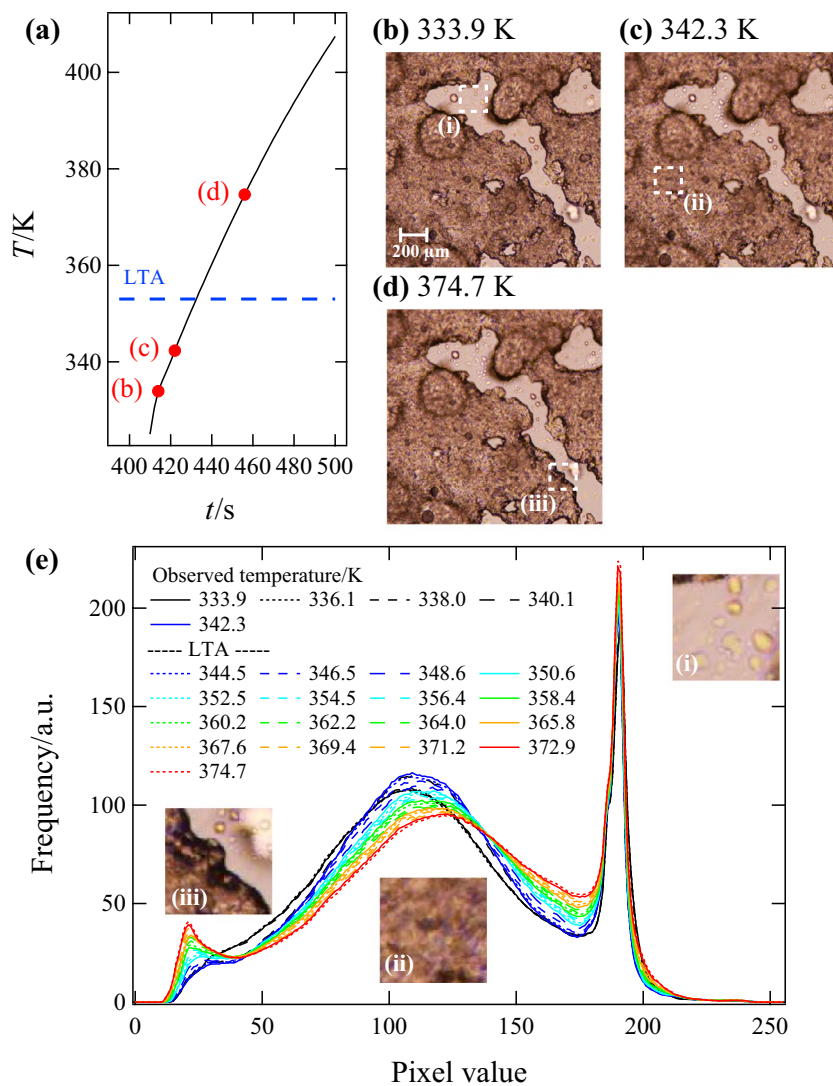
system changed to a uniform liquid (Fig. 7f–i). Therefore, it is concluded that HTA is a process for transition to the liquid state for microcrystals which emerged after the melting of trehalose dihydrate.

On the other hand, we need to draw attention to the morphological changes for the pairs of lowest and highest temperatures at each scan (Fig. 7a–d). Although the differences between those are slightly thinner at the highest temperature, this change is thought to be related to LTA. In the next section, we will conduct a more in-depth analysis of this point.

Morphological changes with LTA

In this section, we discuss the morphological changes accompanied by LTA. The main focus is on the second heating scan, corresponding to the area surrounded by the blue-dotted region in the upper panel of Fig. 7. The specific morphological changes are depicted in Fig. 8. The overall

average brightness is slightly brighter immediately before (Fig. 8c) and after (Fig. 8d) LTA. Although this difference is minimal, the frequency distribution of brightness is taken as we have shown in Sect. 4.3 and is used to analyze the morphological changes associated with the melting of trehalose dihydrate (See, Fig. 5e). Similar to previous results, the outcome for the LTA can also be divided into three regions. Each region represents (i) no material, (ii) the emergence of microcrystals, and (iii) microcrystals are concentrated at the boundary of the liquid state. The variance in (i) with the rise of the temperature is very small, while (ii) and (iii) show significant changes with increasing temperature. In (ii), the peak of the brightness gradually increases with increasing temperature, but its intensity initially increases below LTA and then decreases above LTA. On the other hand, for (iii), although there is very low intensity below LTA, it increased rapidly after LTA.

Fig. 9 The close-up of profiles for the figure analysis with changing temperature for Fig. 8e is shown. **a**, **b** represent profiles around pixel values of 20 (**a**) and 110 (**b**), respectively. **c**, **d** represent the temperature dependence of the intensity for the grayed region in (**a**) and the intensity for the maximum in (**b**), respectively. **e** represents the same figure with Fig. 3b to compare microscopic observation and DSC results. (Color figure online)
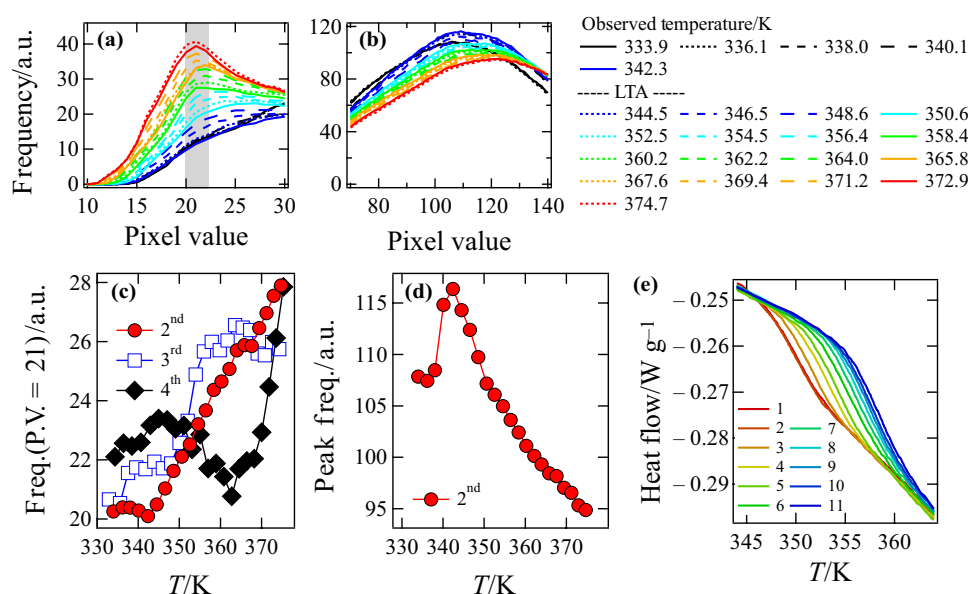
The close-up profile of Fig. 8e should be investigated concerning the variation of temperature. Figure 9a, b indicates close-up profiles of frequencies for second heating scan around the pixel value of 20 and 110, respectively. Where the former is supposed to correspond to the concentrated microcrystals on the boundaries of the liquid surface and the latter to the microcrystals. Then, we assume that the characteristics of the system are elucidated by taking the intensities at the pixel value of 21 for the former case and those at the maximum intensities around the pixel value of 110 for the latter one, respectively, then drawn as Fig. 9c for the former one and Fig. 9d for the latter one, respectively. Here, in the case of Fig. 9c, the results for the thirrd and fourth heating scan are also plotted.

With the interpretation of the kink in Fig. 9c, the number of microcrystals remains constant below LTA, while that grows rapidly above LTA. On the other hand, in case of the Fig. 9d, one possible idea to understand obtained behaviors is gradual increase in brightness that is interpreted as the growth of the size of microcrystals. We would like to say the origin of the change of the intensity that is still an open problem; however, as a whole, above LTA, the amount of microcrystals seems to be increasing.

Comparison with DSC results and microscopic observations

It is worthwhile to compare morphological change and DSC results for LTA. Figure 9c indicates the existence of the hysteresis according to the morphological change. With increase of the number of repetition, the position of the kink is moving to the higher temperature, where it is similar to DSC curve as is indicated in Sect. 4.2 (Fig. 9e). This

correspondence indicates LTA, and morphological change has same origin.

Again, important features to consider in microscopic observation are: 1) the formation of microcrystals immediately after melting of trehalose dihydrate, 2) the disappearance of microcrystals at temperatures higher than the completion of HTA, and 3) the existence of hysteresis for microcrystal growth on temperature variation.

With consideration of 1), since the microcrystals occur above the melting point of trehalose dihydrate, the entity of the microcrystals cannot be a crystal of trehalose dihydrate. Then, this microcrystal should be in a crystalline state of an anhydrous or hydrate with less water fraction than the dihydrate.

Regarding 2), together with a gradual endotherm in between the melting point of trehalose dihydrate and around 430 K in the DSC curve for HTA, the existence of HTA and microcrystals go hand in hand. It means that HTA appears as some kind of melting for the microcrystal structure. This process in microscopic observation is depicted in Fig. 7e, f.

The hysteresis inferred in 3) is particularly important. The increase in microcrystals around T_X shown by microscopic observation (Fig. 9c, d) corresponds to the emergence of LTA shown in the DSC curve.

Discussion and conclusions

Thermal anomalies around 350 K (LTA) and 430 K (HTA) in trehalose dihydrate were comprehensively investigated through thermal measurements using DSC and direct observation using a microscope. Both LTA and HTA were observed only in the direction of the increase in

temperature. We would like to emphasize that this study is the first one to report LTA.

One of the conditions for the occurrence of LTA is to maintain liquid trehalose dihydrate at a temperature lower than the temperature at which HTA is completed (about 430 K). With increasing the temperature to complete HTA, LTA disappeared. The direct microscopic observation demonstrated that HTA is equivalent to a type of melting of spike-like microcrystals above the melting point of trehalose dihydrate. Therefore, the presence of the LTA requires the presence of spike-like microcrystals.

On the other hand, the position of LTA, T_X, was shifted to the higher temperature by the repetition of measurements and by annealing at a higher temperature. Therefore, the growth of the microcrystals is described based on the experienced time of higher temperatures or the duration to anneal. Those treatments push the structure that causes LTA more stabilized and push T_X up to a higher temperature. It should be noted that the liquid state after HTA completion cannot be the same as the liquid state before completion. In fact, after completion of HTA, a clear glass transition was observed around 290 K, which corresponds to a hydrated mixture of trehalose and water at a ratio of 1.4:1.

The phase behavior of trehalose dihydrate inferred from the above is explained using the conceptual diagram as shown in Fig. 10.

1. *Melting of trehalose dihydrate*; trehalose, which was initially in the crystalline state, Crystal I, melts and transitions to the liquid state, Liquid I (Fig. 10a → Fig. 10b).
2. *Coexistence of Liquid I and Crystal II*; immediately after the transition, spike-like microcrystals, called Crystal II, appear from everywhere, forming a coexistence state where Liquid I and Crystals II (Fig. 10b → Fig. 10c).
3. *Melting of Crystal II*; Crystal II gradually melts with increasing temperature (Fig. 10c → Fig. 10d).
4. *Back to a lower temperature*; cooling the system with remaining Crystal II increases the amount of Crystal II (Fig. 10d → Fig. 10e).
5. *LTA*; increasing the temperature larger than the completion of LTA makes the amount of Crystal II increase (Fig. 10e → Fig. 10f).
6. *Melting of Crystal II*; Crystal II gradually melts with increasing temperature as same with process 3 (Fig. 10f → Fig. 10g).
7. *Completion of HTA*; increasing the temperature larger than completion of HTA, Crystal II completely disappeared and turned to Liquid II and thereafter the system does not change even if the temperature is lowered (Fig. 10g → Fig. 10h).

Considering the effect of the hysteresis of repetition of measurements and annealing for LTA, subsequent structural changes in liquid state at high temperature might play an important role, but the detail is not yet clear and remains a further problem in the future.

At last, we would like to discuss the relation between our findings and the origin of the invalidation procedure of cryptobiosis in the polypedilum vanderplanki found by Sakurai et al. [5]. As is discussed in the literature, the temperature to invalidate cryptobiosis is around 350 K and is the same with the temperature where LTA has occurred. Although, the origin of LTA is still not clear, in the process of LTA, the growth of Crystal II has emerged as we have seen. If this process has occurred in the biological tissues, it is easily imagined the growth of crystalline structure might hurt their tissues in that process. Our proposed scenario is one way to explain the process of the emergence

Fig. 10 Schematics of direct microscopical observation throughout experiments. The grayed, light blue, and light green regions represent the crystalline, liquid I, and liquid II states, respectively. The crystalline state appears in (**a**, **c-g**), the liquid I state appears in (**b-g**), and the liquid II state only appears in (**h**). The detailed explanations are shown in the main text. (Color figure online)
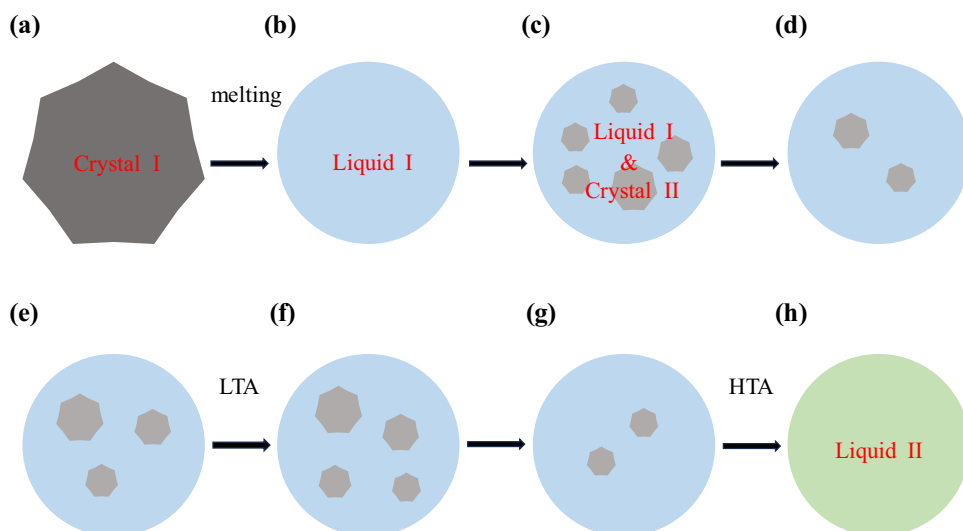
and disappearance of cryptobiosis and in good consistency with current findings.

Author contributions ST contributed to the study's conception and design. KY conducted the first stage of the differential scanning calorimetric measurements, and he was the first to discover the hysteresis for LTA. TY conducted the initial stage of the microscopic measurements, and he was responsible for constructing the experimental setup for the microscopic measurements. RO conducted the rest of the differential scanning calorimetric and microscopic measurements. RO constructed the final form of the experimental setup for microscopic measurements and implementation of the figure analysis for results on the microscopic measurements was achieved. HY and ST advised improving the experimental setup and the direction of the analysis at every moment of the research process. The first draft of the manuscript was written by RO and ST commented on previous versions of the manuscript to sophisticate. All authors read and approved the final manuscript.

References

1. Maruta K, Nakada T, Kubota M, Chaen H, Sugimoto T, Kurimoto M, Tsujisaka Y. Formation of Trehalose from Maltooligosaccharides by a novel enzymatic system. Biosci Biotechnol Biochem. 1995;59(10):1829–34. https://doi.org/10.1271/bbb.59.1829.
2. Richards AB, Krakowka S, Dexter LB, Schmid H, Wolterbeek APM, Waalkens-Berendsen DH, Shigoyuki A, Kurimoto M. Trehalose: a review of properties, history of use and human tolerance, and results of multiple safety studies. Food Chem Toxicol. 2002;40(7):871–98. https://doi.org/10.1016/S0278-6915(02)00011-X.
3. Elbein AD, Pan YT, Pastuszak I, Carroll D. New insights on trehalose: a multifunctional molecule. Glycobiology. 2003;13(4):17–27. https://doi.org/10.1093/glycob/cwg047.
4. Watanabe M, Kikawada T, Minagawa N, Yukuhiro F, Okuda T. Mechanism allowing an insect to survive complete dehydration and extreme temperatures. J Exp Biol. 2002;205(18):2799–802. https://doi.org/10.1242/jeb.205.18.2799.
5. Sakurai M, Furuki T, Akao KI, Tanaka D, Nakahara Y, Kikawada T, Watanabe M, Okuda T. Vitrification is essential for anhydrobiosis in an African chironomid, Polypedilum vanderplanki. Proc Natl Acad Sci USA. 2008;105(13):5093–8. https://doi.org/10.1073/pnas.0706197105.
6. Sakurai M. Experimental and theoretical study on the mechanism of desiccation tolerance of anhydrobiotic organisms induced by Trehalose and LEA. Proteins. 2017;63(1):1–10.
7. McGarvey OS, Kett VL, Craig DQM. An investigation into the crystallization of α,α-trehalose from the amorphous state. J Phys Chem B. 2003;107(27):6614–20. https://doi.org/10.1021/jp0262822.
8. Furuki T, Kishi A, Sakurai M. De- and rehydration behavior of α,α-trehalose dihydrate under humidity-controlled atmospheres. Carbohydr Res. 2005;340(3):429–38. https://doi.org/10.1016/j.carres.2004.12.003.
9. Sussich F, Cesàro A. Trehalose amorphization and recrystallization. Carbohydr Res. 2008;343(15):2667–74. https://doi.org/10.1016/j.carres.2008.08.008.
10. Cesàro A, De Giacomo O, Sussich F. Water interplay in trehalose polymorphism. Food Chem. 2008;106:1318–28. https://doi.org/10.1016/j.foodchem.2007.01.082.
11. Golovina EA, Golovin A, Hoekstra FA, Faller R. Water replacement hypothesis in atomic details: effect of trehalose on the structure of single dehydrated POPC bilayers. Langmuir. 2010;26(13):11118–26. https://doi.org/10.1021/la100891x.
12. Allan M, Chamberlain MC, Mauer LJ. RH-temperature stability diagram of the dihydrate, β-Anhydrate, and α-anhydrate forms of crystalline Trehalose. J Food Sci. 2019;84(6):1465–76. https://doi.org/10.1111/1750-3841.14591.